

# Holographic vector meson melting in a thermal gravity-dilaton background related to QCD

R. Zöllner<sup>1,2</sup> and B. Kämpfer<sup>1,2,a</sup>

<sup>1</sup> Helmholtz-Zentrum Dresden-Rossendorf, 01314 Dresden, Germany

<sup>2</sup> Institut für Theoretische Physik, TU Dresden, 01062 Dresden, Germany

**Abstract.** A holographic model of probe vector mesons (quarkonia) is presented, where the dynamical gravity-dilaton background is adjusted to the thermodynamics of 2 + 1 flavor QCD with physical quark masses. The vector meson action is modified to account for various quark masses. We focus on the  $\Phi$ ,  $J/\psi$  and  $\Upsilon$  meson melting in agreement with hadron phenomenology in heavy-ion collisions at LHC, that is the formation of hadrons at the observed freeze-out temperature of 155 MeV.

## 1 Introduction

Heavy-flavor degrees of freedom receive currently some interest as valuable probes of hot and dense strong-interaction matter produced in heavy-ion collisions at LHC energies. The information encoded, e.g. in quarkonia ( $c\bar{c}$ ,  $b\bar{b}$ ) observables, supplements penetrating electromagnetic probes and hard (jet) probes and the rich flow observables, thus complementing each other in characterizing the dynamics of quarks and gluons up to the final hadronic states (cf. contributions in [1] for the state of the art). Since heavy quarks emerge essentially in early, hard processes, they witness the course of a heavy-ion collision – either as individual entities or subjects of dissociating and regenerating bound states [2,3]. Accordingly, the heavy-quark physics addresses such issues as charm ( $c$ ,  $\bar{c}$ ) and bottom ( $b$ ,  $\bar{b}$ ) dynamics related to transport coefficients [4,5,6,7] in the rapidly evolving and highly anisotropic ambient quark-gluon medium [8,9] as well as  $c\bar{c}$  /  $b\bar{b}$  states as open quantum systems [10,11,12]. The rich body of experimental data from LHC, and also from RHIC, enabled a tremendous refinement of our theoretical treatment which grew up on initiating ideas like “Mott mechanism and the hadronic to quark matter phase transition” [13], “ $J/\psi$  suppression by quark-gluon plasma formation” [14] and “Statistical hadronization of charm in heavy ion collisions at SPS, RHIC and LHC” [15]. For a recent survey on the quarkonium physics we refer the interested reader to [16].

The yields of various hadron species, light nuclei and anti-nuclei – even such ones which are only very loosely bound – emerging from heavy-ion collisions at LHC energies are described by the thermo-statistical model [17] with high accuracy. These yields span an interval of nine orders of magnitude. Refinements have been proposed to resolve the so called proton puzzle and several parameterizations, e.g. related to

---

<sup>a</sup> e-mail: [kaempfer@hzdr.de](mailto:kaempfer@hzdr.de)

excluded volume effects, account for specific inter-hadron forces in the spirit of the Madsen-Bernstein theorem. The final hadrons and nuclear clusters are described by two parameters: the freeze-out temperature  $T_{fo} = 155$  MeV and a freeze-out volume depending on the centrality of the collision. Due to the near-perfect matter-antimatter symmetry at top LHC energies the baryo-chemical potential  $\mu_B$  is exceedingly small,  $\mu_B/T_{fo} \ll 1$ . It is argued in [17] that the freeze-out of color-neutral objects happens just at the demarcation region of hadron matter to quark-gluon plasma, i.e. confinement vs. deconfinement strong-interaction matter. In fact, lattice QCD results [18,19] report a pseudo-critical temperature of  $T_c = 155 \pm 9$  MeV, now further constrained to  $T_c = 156 \pm 1.5$  MeV [20] – a value agreeing with the disappearance of the chiral condensates, a maximum of some susceptibilities and also roughly with the minimum of sound velocity. The key is the adjustment of physical quark masses and the use of 2+1 flavors, in short  $\text{QCD}_{2+1}(\text{phys})$ . Details of the (may be accidental) coincidence of deconfinement and chiral symmetry restoration are matter of debate [21], as also the formation of color-neutral objects out of the cooling quark-gluon plasma at  $T_c$ , in particular also very weakly bound nuclei. Note that at  $T_c$  no phase transition happens, rather the thermodynamics is characterized by a cross-over, e.g. signaled by a pronounced dip in the sound velocity which in turn is related to an inflection point of the pressure as a function of the temperature.

Among the tools for describing hadrons as composite strong-interaction systems is holography. Anchored in the famous AdS/CFT correspondence, holographic bottom-up approaches have facilitated a successful description of mass spectra, coupling/decay strengths etc. of various hadron species. While the direct link to QCD by a holographic QCD-dual or rigorous top-down formulations are still missing, one has to restrict the accessible observables to explore certain frameworks and scenarios. We consider here a scenario which merges (i)  $\text{QCD}_{2+1}(\text{phys})$  thermodynamics described by a dynamical holographic gravity-dilaton background, where the notion "dilaton" refers to a bulk scalar field as conformal symmetry breaker, and (ii) holographic probe vector mesons. We present a scenario which embodies QCD thermodynamics of  $\text{QCD}_{2+1}(\text{phys})$  and the emergence of hadron states at  $T_c$  at the same time. One motivation of our work is the exploration of a (sufficiently simple and thus transparent) holographic model which is in agreement with the above hadron phenomenology in heavy-ion collisions at LHC energies. Early holographic attempts [22,23] to hadrons at non-zero temperatures faced the problem of meson melting at temperatures significantly below the deconfinement temperature  $T_c$ . Several proposals have been made [24] to find rescue avenues which accommodate hadrons at  $T_c$ .

Even though we focus on charmonium and bottomonium we include – for the sake of comparison – the  $\Phi$  meson as strangeonium in our considerations. In the temperature range  $T \approx \mathcal{O}(T_c)$ , the impact of charm and bottom degrees of freedom on the quark-gluon-hadron thermodynamics is minor [25]. Thus, we consider quarkonia as test particles. We follow [26,27,28,29] and model the holographic background by a gravity-dilaton set-up, i.e. without adding further fundamental degrees of freedom (as done, e.g. in [30,31]) to the dilaton, which was originally related solely to gluon degrees of freedom [32]. That is, the dilaton potential is adjusted to  $\text{QCD}_{2+1}(\text{phys})$  lattice data. Such an approach looks quite different in relation to holographic investigations of meson melting without reference to QCD thermodynamics [33,34,35,36,37]. We restrict ourselves to equilibrium and leave non-equilibrium effects [38] for future work.

Our paper is organized as follows. In section 2, the dynamics of the probe vector mesons is formulated and its coupling to the thermodynamics related background is explained. (The recollection of the Einstein-dilaton dynamics is relegated to Appendix A.) Numerical solutions in the strangeness sector ( $\Phi$ ) and charm ( $J/\psi$ ) and bottom ( $\Upsilon$ ) sectors of vector meson states and the melting systematic are dealt with in section 3. We summarize in section 4.

## 2 Probe vector mesons

The action of quarkonia as probe vector mesons in string frame is

$$S_m^V = \frac{1}{k_V} \int d^4x dz \sqrt{g_5} e^{-\phi} G_m(\phi) F^2, \quad (1)$$

where the function  $G_m(\phi(z))$  carries the flavor (or quark-mass, symbolically  $m$ ) dependence and  $F^2$  is the field strength tensor squared of a U(1) gauge field  $\mathcal{A}$  in 5D asymptotic Anti-de Sitter (AdS) space time with the bulk coordinate  $z$  and metric fundamental determinant  $g_5$ ;  $\phi$  is the scalar dilaton field (with zero mass dimension). The structure of (1) is that of a field-dependent gauge kinetic term, familiar, e.g., from realizations of a localization mechanism in brane world scenarios [39,40,41]. In holographic Einstein-Maxwell-dilaton models (cf. [42]), often employed in including a conserved charge density (e.g. [43,44]), such a term refers to the gauge coupling. For the relation to truncated string (M) theory and supergravity, see remarks in [45].

The action (1) with  $G_m = 1$ , originally put forward in the soft-wall (SW) model for light-quark mesons [46], is also used for describing heavy-quark vector mesons [33,34,35], e.g. charmonium [36,37] or bottomonium. As emphasized, e.g. in [36], the holographic background encoded in  $g_5$  and  $\phi$  must be chosen differently to imprint the different mass scales, since (1) with  $G_m = 1$  as such would be flavor blind. Clearly, the combination  $\exp\{-\phi\}G_m(\phi)$  in (1) with flavor dependent function  $G_m(\phi)$  is nothing but introducing effectively a flavor dependent dilaton profile  $\phi_m = \phi - \log G_m$ , while keeping the thermodynamics-steered hadron-universal dilaton  $\phi$ . In fact, many authors use the form  $S_m^V = \frac{1}{k_V} \int d^4x dz \sqrt{g_5} e^{-\phi_m} F^2$  to study the vector meson melting by employing different parameterizations of  $\phi_m$  to account for different flavor sectors. Here, we emphasize the use of a unique gravity-dilaton background for all flavors and include the quark mass (or flavor) dependence solely in  $G_m$ .

Our procedure to determine  $G_m$  is based on the import of information from the hadron sector at  $T = 0$ . The action (1) leads via the gauges  $\mathcal{A}_z = 0$  and  $\partial^\mu \mathcal{A}_\mu = 0$  and the ansatz  $\mathcal{A}_\mu = \epsilon_\mu \varphi(z) \exp\{ip_\nu x^\nu\}$  with  $\mu, \nu = 0, \dots, 3$  and the constant polarization vector  $\epsilon_\mu$  to the equation of motion

$$\varphi'' + \left[ \frac{1}{2} A' + (\partial_\phi \log G_m - 1) \phi' + (\log f)' \right] \varphi' + \frac{p^\mu p_\mu}{f^2} \varphi = 0, \quad (2)$$

where a prime denotes the derivative w.r.t. the bulk coordinate  $z$ ,  $A$  denotes the warp factor and  $f$  is the blackness function of the metric, cf. (12) below. Via the transformation  $\psi(\xi) = \varphi(z(\xi)) \exp\{\frac{1}{2} \int_0^\xi dz \mathcal{S}_T(\xi)\}$  and by introducing the tortoise coordinate  $\xi$  via  $\partial_\xi = (1/f) \partial_z$  one gets eventually the form of a one-dimensional Schrödinger equation with the tortoise coordinate  $\xi$

$$[\partial_\xi^2 - (U_T(z(\xi)) - m^2)] \psi(\xi) = 0, \quad i = 0, 1, 2, \dots \quad (3)$$

with the mass  $m$  in the rest system of the particle given by  $m^2 = p^\mu p_\mu$ . Normalizable solutions in the sense of  $\int_0^\infty |\psi(\xi)|^2 d\xi = 1$  require the boundary conditions  $\psi(0) = 0$  and  $\psi_i(z \rightarrow z_H) = \psi(\xi \rightarrow \infty) \rightarrow 0$ . A detailed analysis of the near-horizon behavior of the solutions of (3) shows that only the trivial solution  $\psi(\xi) = 0$  fulfills the condition  $\psi(z \rightarrow z_H = 0) = 0$  if  $m^2$  is a real number and  $f \neq 1$ , i.e. there are no normalizable solutions except in the case of vanishing temperature. The Schrödinger equivalent potential is

$$U_T \equiv \left( \frac{1}{2} \mathcal{S}'_T + \frac{1}{4} \mathcal{S}_T^2 \right) f^2 + \frac{1}{2} \mathcal{S}_T f f' \quad (4)$$

as a function of  $\xi(z)$  with

$$\mathcal{S}_T \equiv \frac{1}{2}A' - \phi' + \partial_z \log G_m(\phi(z)). \quad (5)$$

At temperatures  $T(z_H) > 0$ ,  $f(z, z_H) \leq 1$ ,  $A = A(z, z_H)$ ,  $\phi = \phi(z, z_H)$ , and the related thermodynamics is given as usual by the Einstein-dilaton bottom-up model (see Appendix A for a recollection). Specifically, a cut-off  $\xi_0$  is needed to ensure

$$\int_{0^+}^{\xi_0} d\xi |\psi(\xi)|^2 = 1. \quad (6)$$

We employ here  $z(\xi_0) = z_H(1 - \tilde{\epsilon})$  with  $\tilde{\epsilon} = 10^{-2}$ .

At  $T = 0$  (label “0”),  $f = 1$  and  $\xi = z$  and  $U_T = U_0$  with

$$U_0(z) \equiv \frac{1}{2}\mathcal{S}'_0 + \frac{1}{4}\mathcal{S}_0^2 \quad (7)$$

$$\mathcal{S}_0 \equiv \frac{1}{2}A'_0(z) - \phi'_0(z) + \partial_z \log G_m(\phi(z)), \quad (8)$$

and (3) becomes

$$[\partial_z^2 + (U_0(z) - m_i^2)] \psi_i = 0 \quad (9)$$

again with the normalizing conditions  $\psi_i(0) = 0$  and  $\psi_i(z \rightarrow \infty) \rightarrow 0$ , but this time without the necessity of introducing a cut-off.

That is, at  $T = 0$  one has to deal with a suitable Schrödinger equivalent potential  $U_0(z)$  to generate the wanted spectrum  $m_i$ . In such a way, the needed hadron physics information at  $T = 0$  is imported and included in  $U_0$ . The next step is solving (7) with the initial condition  $\mathcal{S}_0(z \rightarrow 0) \rightarrow -\frac{1}{z}$  (coming from the asymptotic AdS geometry in combination with (8)) by numerical means in general, since it is a Riccati equation, to obtain  $\mathcal{S}_0(z)$  and, with (8), then  $G_m(\phi)$  with  $G_m(0) = 1$ . This needs  $A'_0(z)$  and  $\phi'_0(z)$ , which follow from the thermodynamics sector in Appendix A via  $A_0 = A(z) = \lim_{z_H \rightarrow \infty} A(z, z_H)$  and  $\phi_0 = \phi(z) = \lim_{z_H \rightarrow \infty} \phi(z, z_H)$ . One has to suppose that these limits are meaningful. The limited information from lattice QCD thermodynamics (both in temperature and in accuracy) may pose here a problem. Ignoring such a potential obstacle we use then  $G_m(\phi) = G_m(z(\phi_0))$  as universal (i.e. temperature independent) function to analyze (3) with (4, 5) at non-zero temperature.

### 3 Systematic of quarkonia melting: Exploring a two-parameter ansatz of $U_0$

Our setting does not explicitly refer to a certain quark mass  $m$ . Instead, an ansatz  $U_0(z, \mathbf{p})$  with parameter n-tuple  $\{\mathbf{p}\}$  is used such to catch a certain quarkonium mass spectrum. Insofar,  $m$  is to be considered as cumulative label highlighting the dependence of  $G_m$  on a parameter set which originally enters  $U_0$ .

A simple two-parameter ansatz for  $U_0(z)$  is [36]

$$L^2 U_0(z) = \frac{3}{4} \left( \frac{L}{z} \right)^2 + a^2 \left( \frac{z}{L} \right)^2 + 4b \quad (10)$$

which is known to deliver via (9) the normalizable functions  $\psi_i$  with discrete eigenvalues

$$L^2 m_i^2 = 4(a + b + i a), \quad i = 0, 1, 2, \dots \quad (11)$$

Clearly, (10) is a slight modification of the SW model ansatz [46] with  $\frac{3}{4z^2}$  stemming from the warp factor  $A(z)$  and  $z^2$  emerging from a quadratic dilaton profile. Note the Regge type excitation spectrum  $m_i^2 = m_0^2 + ia/L^2$  with intercept and slope to be steered by two independent parameters  $a$  and  $b$ . The level spacing (referring to masses squared!) is  $L^2(m_1^2 - m_0^2) = 4a$ , meaning  $m_1^2 > 2m_0^2$  for  $a > \frac{1}{4}L^2m_0^2$ . In other words, requesting small level spacing w.r.t. the ground state mass  $m_0^2 = 4(a+b)/L^2$  implies selecting smaller values of  $a$ .

As we shall demonstrate below, the ansatz (10) has several drawbacks and, therefore, is to be considered only as illustrative example. For instance, the sequence of radial  $\mathcal{Y}$  excitations in nature does not form a linear Regge trajectory [47]. This prevents a unique mapping of  $m_{0,1} \rightarrow (a, b)$ . While the radial excitations of  $J/\psi$  follow quite accurately a linear Regge trajectory in nature [47], the request of accommodating further  $J/\psi$  properties in  $U_0$  calls also for modifying (10), cf. [36]. Despite the mentioned deficits, the appeal of (10, 11) is nevertheless the simply invertible relation  $m_i^2(a, b)$  yielding  $a(m_{0,1})$  and  $b(m_{0,1})$ . Since we are going to study the systematic, we keep the primary parameters  $a$  and  $b$  in what follows.

Instead of discussing results at isolated points in parameter space referring to  $\Phi$ ,  $J/\psi$  and  $\mathcal{Y}$  ground states  $m_0$  and first excited states  $m_1$ , we consider the systematic over the  $a$ - $b$  plane. We define as dissociation temperatures  $T_{dis}^{g.s.,1st}(z_H)$  such values, at which the ground state or first excited state cannot longer be accommodated in the Schrödinger equivalent potential  $U_T$ . At  $T > T_{dis}^{g.s.}$  and  $T > T_{dis}^{1st}$ , the ground state or the first excited state are called “molten” or “dissociated” since the respective normalizable solutions of (3) in the sense of (6) do not exist. One might call  $T_{dis}$  also break-up temperature. We emphasize however as an aside that, in some significant temperature range above  $T_{dis}^{g.s.}$ , the spectral functions of  $J/\psi$  and  $\mathcal{Y}$  display still clearly observably peaks despite the failure of  $U_T$  to accommodate normalizable states via the Schrödinger equation (3). These peaks, albeit not longer spikes, obey thermal shifts and thermal broadening with increasing temperature until approaching a smooth continuum at a certain temperature  $T_{peak-dis} > T_{dis}^{g.s.}$ . Such a behavior could be interpreted as pre-formation of modes which turn upon cooling into the corresponding quasi-particles at lower temperatures. We leave the investigation of spectral functions to separate follow-up work and focus on implications of (3) - (10).

A survey of  $T_{dis}^{g.s.}(a, b)$  is exhibited in Fig. 1-left by the solid curves. The dashed curves depict the loci of  $m_0(a, b) = 1.019$  GeV ( $\Phi$ ), 3.097 GeV ( $J/\psi$ ) and 9.46 GeV ( $\mathcal{Y}$ ). The two-parameter ansatz (10) allows for an independent fixing of  $m_1(a, b) = 1.68$  GeV ( $\Phi_{1680}$ ), 3.686 GeV ( $\psi(2S)$ ) and 10.0234 GeV ( $\mathcal{Y}(2S)$ ), which adds a further congruence of curves (thin dotted). At the intersections of the respective curves  $m_0(a, b)$  and  $m_1(a, b)$ , the parameter doublets  $(a, b)$  would exactly correspond to the PDG values. It turns out, however, that the dissociation temperatures would be too low in such a case. Instead of keeping  $m_1$  at PDG values, we allow for larger spacings and thus get larger dissociation temperatures at given  $m_0$ . Note that, according to the thermo-statistical hadronization model [17],  $T_{dis} \geq 155$  MeV is required for all (ground state) hadron species – otherwise the impressive coverage of hadron abundances ranging over nine orders of magnitude would be hardly understandable.

Employing the QCD-related thermal background is quantitatively important. If we use the schematic background parameterized by  $A(z, z_H) = -2 \log(z/L)$ ,  $f(z, z_H) = 1 - (z/z_H)^4$ ,  $\phi(z, z_H) = (z/L)^2$ , the quarkonia break-up curves  $T_{dis}^{g.s.}$  are shifted to right-down, see Fig. 1-right. Nevertheless, the overall pattern is governed by the utilized ansatz  $U_0(z; a, b)$ .

To understand the reason of the variation of  $T_{dis}^{g.s.}(a, b)$  let us consider the Schrödinger equivalent potentials  $U_{0,T}$  for three points  $(a, b)$  in the parameter space which correspond to  $T_{dis}^{g.s.} = 100, 150$  and 200 MeV and given values  $m_0(\Phi, J/\psi, \mathcal{Y}) = const.$

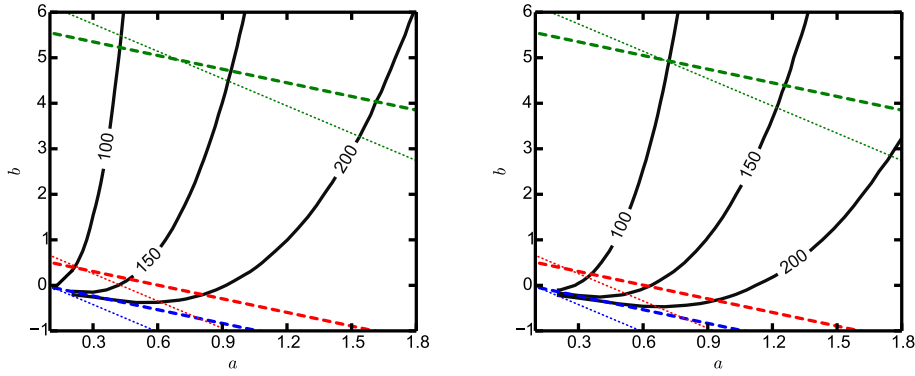


**Fig. 1.** Contour plot of  $T_{dis}^{g.s.}$  (in MeV) over the  $a$ - $b$  plane (solid labeled curves). Also depicted are the curves  $m_0(a, b) = m_{g.s.}(\Phi, J/\psi, \Upsilon)$  (dashed) and  $m_1(a, b) = m_{1st}(\Phi, J/\psi, \Upsilon)$  (dotted) with the color code  $\Phi$ -blue,  $J/\psi$ -red and  $\Upsilon$ -green. Left panel: using the background adapted to QCD<sub>2+1</sub>(phys) (see Appendix A), right panel: using a schematic background with  $A(z, z_H) = -2 \log(z/L)$ ,  $f(z, z_H) = 1 - (z/z_H)^4$ , and  $\phi(z, z_H) = (z/L)^2$ . Scale setting by  $L^{-1} = 1.99$  GeV.

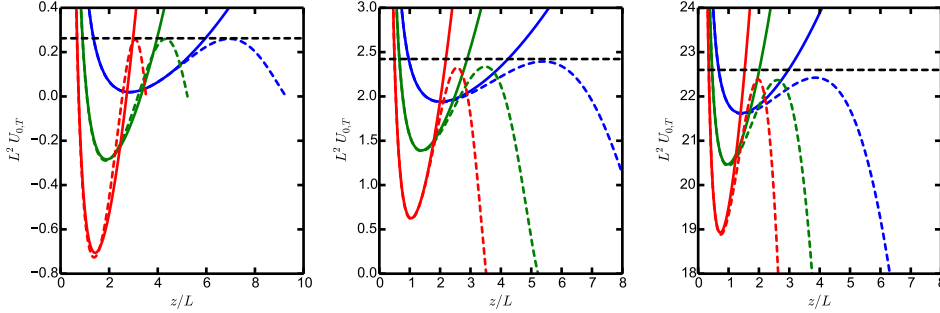


**Fig. 2.** The Schrödinger equivalent potentials  $U_0$  (solid curves) and  $U_T$  (dashed curves) as a function of  $z$  for  $\Phi$  (left),  $J/\psi$  (middle) and  $\Upsilon$  (right). The horizontal lines mark the respective ground states at  $T = 0$ . The parameters  $(a, b)$  correspond to the crossing points of the curves  $m_0(a, b)$  with the dissociation temperatures  $T_{dis}^{g.s.} = 100$  MeV (blue), 150 MeV (green) and 200 MeV (red), cf. Fig. 1. These temperatures are related via the relation  $LT(z_H)$ , exhibited in Fig. 5-right, to the horizon position  $z_H$ . Note that  $U_T(z, z_H)|_{z=z_H} = 0$  due to  $f(z, z_H)|_{z=z_H} = 0$  in (4).

The essence is that going on a curve  $m_0(a, b) = const$  to the right, i.e. keeping the ground state mass constant and enlarging  $a$ , thus consecutively crossing the curves  $T_{dis}^{g.s.} = 100, 150, 200$  MeV, the Schrödinger equivalent potential  $U_0$  and thus  $U_T$  become deformed in a characteristic manner from a shallow shape (small  $a$ ) to a squeezed shape (large  $a$ ), see Fig. 2. Thus, at a certain value of  $z_H$  – corresponding to the temperature  $T(z_H)$  – the shallower Schrödinger equivalent potential might not accommodate the ground state, while the squeezed and deeper potential can do so. Analog features are met for excited states. These observations offer an avenue for the design of suitably improved parameterizations of  $U_0$ , e.g. by introducing a pronounced dip at small values of  $z$ , as used in [33,34,35,36,37].

The ansatz (10) facilitates a sequential melting upon increasing temperature,  $T_{dis}^{g.s.} > T_{dis}^{1st} > T_{dis}^{2nd}$  etc., and allows potentially for a strong flavor dependence

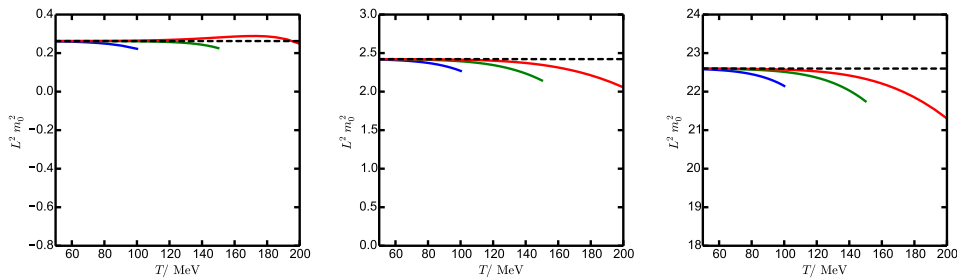


**Fig. 3.** The dependence of the ground state masses  $L^2 m_0^2$  of  $\Phi$  (left panel),  $J/\psi$  (middle panel) and  $\Upsilon$  (right panel) on the temperature  $T$  for the same parameter doublets  $(a, b)$  and color codes as Fig. 2. The horizontal dashed lines depict the respective  $T = 0$  values. The same ordinate scales as in Fig. 2 are displayed.

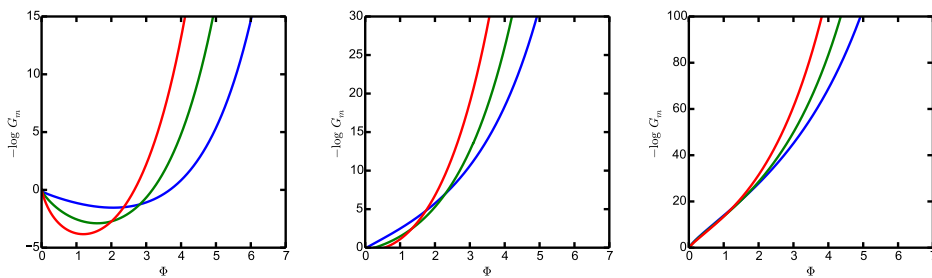


**Fig. 4.** The quantities  $-\log G_m(\phi)$  for the same parameter selection scheme as in Figs. 2 and 3.  $\Phi$ : left pane,  $J/\psi$ : middle panel, and  $\Upsilon$ : right panel.

$T_{dis}^{g.s.}(\Upsilon) > T_{dis}^{g.s.}(J/\psi) > T_{dis}^{g.s.}(\Phi)$ . Furthermore, the variation of  $U_T$  as a function of the temperature causes a *negative* mass shift, see Fig. 3. Such thermal mass shifts are employed in [7] to pin down the heavy-quark (HQ) transport coefficient  $\gamma$  which can be considered as the dispersive counterpart of the HQ momentum diffusion coefficient  $\kappa = 2T^3/(DT)$ , where  $D$  stands for the HQ spatial diffusion coefficient. Reference [16] stresses the tension within previous holographic results [37], where *positive* mass shifts are reported, in contrast to *negative* shifts, e.g. in [35]. Our set-up does not resolve that issue on a firm basis, since the thermal mass shifts of  $J/\psi$  and  $\Upsilon$  in Fig. 3 are noticeably larger than the lattice QCD-based values quoted in [7]. In addition, the sign of the thermal mass shift can depend on the actual parameters  $a$  and  $b$  in the model Eq. (10) as evidenced in the left panel of Fig. 3. However, the  $\Phi$  meson should be considered neither as a HQ representative nor as a proper probe due to missing back-reaction in our setting.

Finally, we exhibit in Fig. 4 the quantity  $-\log G_m$  as a function of  $\phi$  with the same selection scheme of the parameters  $(a, b)$  as in Figs. 2 and 3. Note the huge variation of  $G_m(\phi)$  and the very strong flavor dependence.

## 4 Summary

In summary we introduce a modification of the holographic vector meson action for quarkonia such to join (i) the  $\text{QCD}_{2+1}(\text{phys})$  thermodynamics, described solely by a dilaton and the metric coefficients, with (ii) a Regge type spectrum at zero temperature. The vector mesons belong to different Regge trajectories, e.g. the quarkonia

$J/\psi$  and  $\Upsilon$  and  $\Phi$  as well. The formal construction is based on an effective dilaton  $\phi_m = \phi - \log G_m$ , where  $\phi$  is solely tight to the thermodynamics background, while the flavor dependent quantity  $G_m$  is determined by a combination of  $\phi$  and the adopted Schrödinger equivalent potential. The later one can be chosen with much sophistication to accommodate many hadron properties. We use here only a two-parameter shape to demonstrate features of our scheme, where the thermodynamic background at  $T > 0$  and meson spectra at  $T = 0$  serve as input to analyze the quarkonia melting at  $T > 0$ . According to the hadron and nuclear phenomenology at LHC [17], hadrons must exist at and below temperatures  $T_c \approx T_{fo} \approx 155$  MeV. Ideally, the light hadrons, represented in our approach by  $\Phi$  mesons as vector probe states, should form upon cooling at  $T_c$ , while charmonium or bottomonium must have higher melting temperatures according to QCD results [48,49]. Our holographic set-up is a purely static one, i.e. “meson melting” is meant as a determination of the dissociation or break-up temperature, rather than a dynamical process.

The authors gratefully acknowledge the collaboration with J. Knaute and thank M. Ammon, D. Blaschke, M. Kaminski and K. Redlich for useful discussions. The work is supported in part by STRONG2020.

## A Gravity-dilaton background

Deforming the AdS metric by putting a Black Hole with horizon at  $z_H$  yields the metric for the infinitesimal line elements squared

$$ds^2 = \exp\{A(z, z_H)\} \left[ f(z, z_H) dt^2 - dx^2 - \frac{dz^2}{f(z, z_H)} \right], \quad (12)$$

where  $f(z, z_H)|_{z=z_H} = 0$  is a simple zero. Identifying the Hawking temperature  $T(z_H) = -\partial_z f(z, z_H)|_{z=z_H}/4\pi$  with the temperature of the system at bulk boundary  $z \rightarrow 0$ , and the attributed Bekenstein-Hawking entropy density  $s(z_H) = \frac{2\pi}{\kappa} \times$

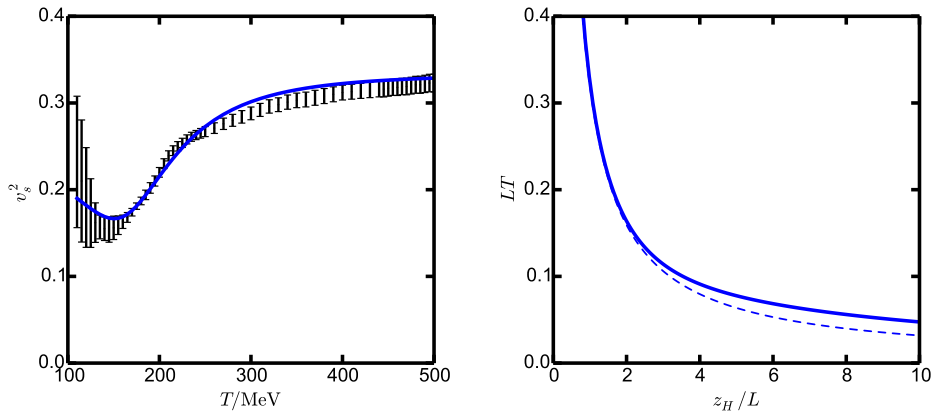


**Fig. 5.** Adjustment of the dilaton potential (14) to lattice QCD data [18,19], in particular, to the velocity of sound squared,  $v_s^2 = \frac{d \log T}{d \log s}$  as a function of temperature (left panel). Note that the dip in sound velocity is characteristic for the cross-over. The resulting temperature  $LT(z_H)$  as a function of  $z_H/L$  is exhibited in the right panel by the solid curve; the dashed curve is for  $T(z_H) = 1/\pi z_H$ .



$\exp\{\frac{3}{2}A(z, z_H)|_{z=z_H}\}$  one describes holographically the thermodynamics.  $f = 1$  at  $T = 0$  is attributed to vacuum. The gravity-dilaton background is determined by the action in the Einstein frame

$$S = \frac{1}{2\kappa} \int d^4x dz \sqrt{g_5} \left[ R - \frac{1}{2}(\partial_z \phi)^2 - V(\phi) \right], \quad (13)$$

where  $R$  stand for the curvature invariant and  $\kappa = 8\pi G_5$ . (For our purposes, the numerical values of  $\kappa$  and  $G_5$  as well as  $k_V$  in (1) are irrelevant.) The dilaton potential  $V(\phi)$  is the central quantity [29]. We use a simple three-parameter ansatz

$$-L^2 V = 12 \cosh(\gamma\phi) + \phi_2 \phi^2 + \phi_4 \phi^4 \quad (14)$$

to find from the field equations and equation of motion for the metric (12)

$$A'' = \frac{1}{2}A'^2 - \frac{1}{3}\phi'^2, \quad (15)$$

$$f'' = -\frac{2}{3}A'f', \quad (16)$$

$$\phi'' = -\left(\frac{2}{3}A' + \frac{f'}{f}\right)\phi' + \frac{1}{f}e^A \partial_\phi V \quad (17)$$

the suitable coefficients  $(\gamma, \phi_2, \phi_4) = (0.568, -1.92, -0.04)$  together with  $L^{-1} = 1.99$  GeV which deliver a satisfactory description of the lattice QCD<sub>2+1</sub>(phys) data [18,19], see Fig. 5. The prime means differentiation w.r.t.  $z$  in (15) - (17), and boundary conditions are  $A(z \rightarrow 0) \rightarrow -2 \log(z/L)$ ,  $\phi(0) = 0$ ,  $\phi'(0) = 0$ ,  $f(0) = 1$ ,  $f(z_H) = 0$ . Despite the conformal dimension  $\Delta$  (from  $\Delta(\Delta - 4) = L^2 m_\phi^2$  leading to  $\Delta = 2 + \sqrt{4 - 2\phi_2 - 12\gamma^2} = 3.9$ ) of the dual operator to  $\phi$  is not four, we denote here the bulk scalar field  $\phi$  as “dilaton”, thus following the nomenclature, e.g. in [27,28,43].

## References

1. F. Antinori, A. Dainese, P. Giubellino, V. Greco, M. P. Lombardo and E. Scomparin, Nucl. Phys. A **982**, pp.1 (2019).
2. F. Prino and R. Rapp, J. Phys. G **43**, no. 9, 093002 (2016)
3. X. Yao and B. Müller, Phys. Rev. D **100**, no. 1, 014008 (2019)
4. R. Rapp *et al.*, Nucl. Phys. A **979**, 21 (2018)
5. Y. Xu *et al.*, Phys. Rev. C **99**, no. 1, 014902 (2019)
6. S. Cao *et al.*, Phys. Rev. C **99**, no. 5, 054907 (2019)
7. N. Brambilla, M. A. Escobedo, A. Vairo and P. Vander Griend, Phys. Rev. D **100**, no. 5, 054025 (2019)
8. C. Chattopadhyay and U. W. Heinz, Phys. Lett. B **801**, 135158 (2020)
9. D. Bazow, U. W. Heinz and M. Strickland, Phys. Rev. C **90**, no. 5, 054910 (2014)
10. R. Katz and P. B. Gossiaux, Annals Phys. **368**, 267 (2016)
11. J. P. Blaizot and M. A. Escobedo, Phys. Rev. D **98**, no. 7, 074007 (2018)
12. N. Brambilla, M. A. Escobedo, J. Soto and A. Vairo, Phys. Rev. D **97**, no. 7, 074009 (2018)
13. D. Blaschke, F. Reinholz, G. Ropke and D. Kremp, Phys. Lett. B **151**, 439 (1985).
14. T. Matsui and H. Satz, Phys. Lett. B **178**, 416 (1986).
15. A. Andronic, P. Braun-Munzinger, K. Redlich and J. Stachel, Phys. Lett. B **571**, 36 (2003)
16. A. Rothkopf, Phys. Rept. **858**, 1 (2020)
17. A. Andronic, P. Braun-Munzinger, K. Redlich and J. Stachel, Nature **561**, no. 7723, 321 (2018)

18. S. Borsanyi, Z. Fodor, C. Hoelbling, S. D. Katz, S. Krieg and K. K. Szabo, Phys. Lett. B **730**, 99 (2014)
19. A. Bazavov *et al.* [HotQCD Collaboration], Phys. Rev. D **90**, 094503 (2014)
20. A. Bazavov *et al.* [HotQCD Collaboration], Phys. Lett. B **795**, 15 (2019)
21. H. Suganuma, T. M. Doi, K. Redlich and C. Sasaki, J. Phys. G **44**, 124001 (2017)
22. P. Colangelo, F. Giannuzzi and S. Nicotri, JHEP **1205**, 076 (2012)
23. P. Colangelo, F. Giannuzzi and S. Nicotri, Phys. Rev. D **80**, 094019 (2009)
24. R. Zöllner and B. Kämpfer, Phys. Rev. C **94**, no. 4, 045205 (2016)
25. S. Borsanyi *et al.*, Nature **539**, no. 7627, 69 (2016)
26. S. S. Gubser and A. Nellore, Phys. Rev. D **78**, 086007 (2008)
27. S. I. Finazzo, R. Rougemont, H. Marrochio and J. Noronha, JHEP **1502**, 051 (2015)
28. S. I. Finazzo and J. Noronha, Phys. Rev. D **89**, no. 10, 106008 (2014)
29. R. Zöllner and B. Kämpfer, Eur. Phys. J. Plus **135**, 304 (2020)
30. S. P. Bartz and T. Jacobson, Phys. Rev. D **94**, 075022 (2016)
31. S. P. Bartz and J. I. Kapusta, Phys. Rev. D **90**, no. 7, 074034 (2014)
32. U. Gursoy, E. Kiritsis, L. Mazzanti, G. Michalogiorgakis and F. Nitti, Lect. Notes Phys. **828**, 79 (2011)
33. N. R. F. Braga, M. A. Martin Contreras and S. Diles, Eur. Phys. J. C **76**, no. 11, 598 (2016)
34. N. R. F. Braga and L. F. Ferreira, Phys. Rev. D **94**, no. 9, 094019 (2016)
35. M. Fujita, T. Kikuchi, K. Fukushima, T. Misumi and M. Murata, Phys. Rev. D **81**, 065024 (2010)
36. H. R. Grigoryan, P. M. Hohler and M. A. Stephanov, Phys. Rev. D **82**, 026005 (2010)
37. N. R. F. Braga, L. F. Ferreira and A. Vega, Phys. Lett. B **774**, 476 (2017)
38. L. Bellantuono, P. Colangelo, F. De Fazio, F. Giannuzzi and S. Nicotri, Phys. Rev. D **96**, no. 3, 034031 (2017)
39. A. E. R. Chumbes, J. M. Hoff da Silva and M. B. Hott, Phys. Rev. D **85**, 085003 (2012)
40. M. Eto and M. Kawaguchi, JHEP **1910**, 098 (2019)
41. M. Arai, F. Blaschke, M. Eto and N. Sakai, Phys. Rev. D **96**, no. 11, 115033 (2017)
42. O. DeWolfe, S. S. Gubser and C. Rosen, Phys. Rev. D **83**, 086005 (2011)
43. R. Rougemont, A. Ficnar, S. Finazzo and J. Noronha, JHEP **1604**, 102 (2016)
44. J. Knaute, R. Yaresko and B. Kämpfer, Phys. Lett. B **778**, 419 (2018)
45. S. S. Gubser and F. D. Rocha, Phys. Rev. D **81**, 046001 (2010)
46. A. Karch, E. Katz, D. T. Son and M. A. Stephanov, Phys. Rev. D **74**, 015005 (2006)
47. D. Ebert, R. N. Faustov and V. O. Galkin, Eur. Phys. J. C **71**, 1825 (2011)
48. R. Larsen, S. Meinel, S. Mukherjee and P. Petreczky, Phys. Lett. B **800**, 135119 (2020)
49. S. Kim, P. Petreczky and A. Rothkopf, JHEP **1811**, 088 (2018)